



Constraining the Source of the M_w 8.1 Chiapas, Mexico Earthquake of 8 September 2017 Using Teleseismic and Tsunami Observations

MOHAMMAD HEIDARZADEH,¹ TAKEO ISHIBE,² and TOMOYA HARADA³

Abstract—The September 2017 Chiapas (Mexico) normal-faulting intraplate earthquake (M_w 8.1) occurred within the Tehuantepec seismic gap offshore Mexico. We constrained the finite-fault slip model of this great earthquake using teleseismic and tsunami observations. First, teleseismic body-wave inversions were conducted for both steep (NP-1) and low-angle (NP-2) nodal planes for rupture velocities (V_r) of 1.5–4.0 km/s. Teleseismic inversion guided us to NP-1 as the actual fault plane, but was not conclusive about the best V_r . Tsunami simulations also confirmed that NP-1 is favored over NP-2 and guided the $V_r = 2.5$ km/s as the best source model. Our model has a maximum and average slips of 13.1 and 3.7 m, respectively, over a 130 km \times 80 km fault plane. Coulomb stress transfer analysis revealed that the probability for the occurrence of a future large thrust interplate earthquake at offshore of the Tehuantepec seismic gap had been increased following the 2017 Chiapas normal-faulting intraplate earthquake.

Key words: Pacific ocean, tsunami, 2017 Chiapas earthquake, tsunami modeling, teleseismic body-wave inversion, Coulomb stress transfer.

1. Introduction

Offshore Chiapas, Mexico, experienced a great M_w (moment magnitude) 8.2 intraplate tsunamigenic earthquake on 8 September 2017 according to the United States Geological Survey (USGS). The earthquake occurred in 93.899°W and 15.022°N at 04:49:19 UTC having a depth of 47.4 km (Fig. 1)

according to the USGS. Our study resulted in an M_w 8.1 for this earthquake which is used hereafter. The epicenter was located at a distance of 104 km to the southwest of Pijijiapan in Chiapas province; hence, this earthquake is also known as the Pijijiapan earthquake. Both the USGS and the Global CMT (GCMT) reported a normal-faulting mechanism solution for this earthquake: strike angle, 314°; dip angle, 73°; rake angle, -100° from the USGS and the respective values of 320°, 77° and -92° from the GCMT. Being comparable to the 1932 M_w 8.2 Jalisco earthquake (Fig. 1b), the Chiapas earthquake has been widely referred to as the largest event in a century in this region. Ninety-eight deaths and more than 300 people injured were reported following the 2017 earthquake. A moderate tsunami was generated whose coastal height was reported around 3 m (Ramírez-Herrera et al. 2018). The earthquake was not capable of generating a powerful tsunami because it was relatively deep. The earthquake source model of this event was studied by Gusman et al. (2018) and Adriano et al. (2018) through tsunami inversions. Ramírez-Herrera et al. (2018) performed a field survey of the tsunami.

From the regional tectonic point of view, the Chiapas earthquake occurred within the North American Plate at ~ 100 km from the Middle America Trench where the Cocos Plate is subducting beneath the North American Plate (Fig. 1b). As shown in Fig. 1b, the epicentral area is located within a seismic gap zone along offshore Mexico, which is called the Tehuantepec gap (e.g., Singh et al. 1981). Based on the USGS catalog, 38 $M > 7$ earthquakes were recorded in this subduction zone including 15 tsunamigenic events (Fig. 1b) (Hatori 1995). The latest notable tsunamis in this region were generated

Electronic supplementary material The online version of this article (<https://doi.org/10.1007/s00024-018-1837-6>) contains supplementary material, which is available to authorized users.

¹ Department of Civil and Environmental Engineering, Brunel University London, Uxbridge UB8 3PH, UK. E-mail: mohammad.heidarzadeh@brunel.ac.uk

² Association for the Development of Earthquake Prediction, Tokyo, Japan.

³ Earthquake Research Institute, the University of Tokyo, Tokyo, Japan.

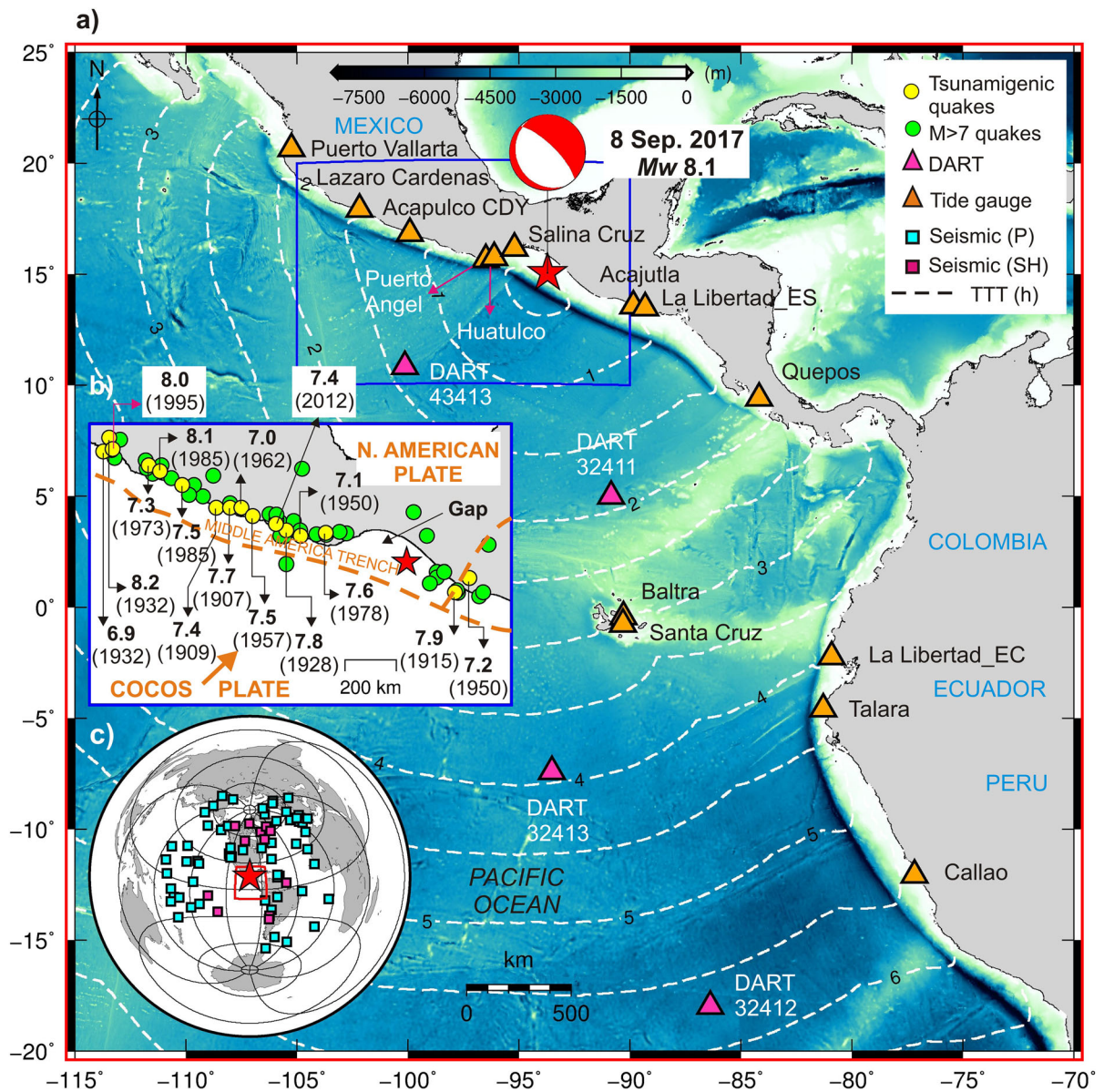


Figure 1

a The epicenter of the 8 September 2017 M_w 8.1 Chiapas, Mexico earthquake (red star) and the locations of tsunami observation stations (tide gauge and DART stations). Tsunami travel times (TTT in hours) are indicated by white-dashed lines. **b** Epicenters of $M > 7$ earthquakes (green and yellow circles) since 1900 AD, as retrieved from the USGS earthquake catalog along with those of tsunamigenic events (yellow circles) from Hatori (1995). **c** Seismic observation stations for teleseismic P (cyan) and SH (pink) waves used in this study

following the M_w 8.0 thrust earthquake on 9 October 1995 (Ortiz et al. 1998; Synolakis and Okal 2005), M 7.6 earthquake on 21 September 1985 (Ortiz et al. 2000; Okal and Synolakis 2004) (M 7.5 as reported by Hatori 1995) and M 7.6 thrust earthquake on 29 November 1978 (Singh et al. 1980) (Fig. 1b).

The recent 2017 Chiapas event is important because it is the first significant tsunami along the Mexican coast in the past 22 years (since 1995). A small tsunami was reported in this region following the 20 March 2012 M_w 7.4 earthquake (M.T. Ramirez-Herrera; written communications). In

addition, it is a tsunami event generated by a steep normal-faulting earthquake which is not frequent. The other recent tsunamis generated by normal-faulting earthquakes occurred offshore Solomon Islands on 18 July 2015 (M_w 7.0) (Heidarzadeh et al. 2016b), offshore Kuril Islands in 2007 (Rabinovich et al. 2008; Fujii and Satake 2008) and offshore Fukushima (Japan) on 21 November 2017 (Gusman et al. 2017). The purposes of this study are: 1) to constrain the finite-fault slip model of the 2017 Chiapas earthquake using teleseismic and tsunami observations, and 2) to investigate changes in the Coulomb stress for the Tehuantepec gap region. The source model obtained in this study helps understand future earthquake and tsunami hazards offshore Mexico and adds to the existing knowledge on tsunami genesis of normal-faulting earthquakes.

2. Data and Methods

The data employed here were 18 tsunami (Fig. 1a) and 76 teleseismic body-wave records (Fig. 1c). Among 18 tsunami records, 4 were deep-ocean assessment and reporting of tsunamis (DART) records, downloaded from the US National Oceanic and Atmospheric Administration website (<http://www.ndbc.noaa.gov/dart.shtml>), and 14 were tide gauge records provided by the Intergovernmental Oceanographic Commission (<http://www.ioc-sealevelmonitoring.org/>) and the Mexican Servicio Mareográfico Nacional (<http://www.mareografico.unam.mx/portal/>). All tsunami observations had a sampling interval of 1 min. The tidal signals were estimated by a polynomial-fitting approach and were then subtracted from the original tsunami observation to produce tsunami waveforms. The 76 dataset of teleseismic records include 64 P and 12 SH waves. These data belonged to distances 30° – 100° from the epicenter (Fig. 1) and were retrieved from the Data Management Center of the Incorporated Research Institutions for Seismology (IRIS; <https://www.iris.edu/hq/>). All teleseismic data were filtered in the frequency band range of 0.004–1.0 Hz and were deconvolved into the ground displacements. The duration of the waveforms used in the teleseismic inversion was 90 s from the calculated P or SH wave

arrival times. The velocity structures used in this study were based on CRUST 1.0 (Laske et al. 2013) and ak135 (Kennett et al. 1995).

The 2003 Kikuchi and Kanamori's teleseismic body-wave inversion program (<http://www.eri.u-tokyo.ac.jp/etal./KIKUCHI/>) was applied for estimating the finite-fault slip model. Both nodal planes (NP) (steep and low-angle faults with dip angles of 77° and 13° ; called hereafter as NP-1 and NP-2, respectively) from the GCMT focal solution were examined to investigate which nodal plane better explained the waveform data. We used subfaults with length and width of 10 km (along strike and dip) over the total extent of 100–130 km for teleseismic inversion by allowing maximum rupture duration of 9.5 s for each subfault. Six rise-time triangles were used and each triangle had a duration of 3 s overlapped by 1.5 s with the neighboring triangles. The rupture velocity (V_r) was varied from 1.5 to 4.0 km/s with 0.5 km/s intervals; therefore, 12 slip distributions were estimated using teleseismic inversions: 6 for NP-1 and the other 6 for NP-2. The reason for producing 12 slip distributions was to investigate which nodal plane (i.e., NP-1 or NP-2) and which V_r better reproduced the teleseismic and tsunami observations. As reported by various authors (e.g., Lay et al. 2014; Gusman et al. 2015; Zhang et al. 2017; Heidarzadeh et al. 2016a, 2017a), the results of teleseismic inversions are not unique due to the uncertainties associated with V_r and therefore they need to be constrained by other types of observations such as tsunami observations.

The numerical package of Satake (1995) was employed for simulations of tsunami propagation on the bathymetry data provided by GEBCO-2014 (The General Bathymetric Chart of the Oceans) digital atlas having a resolution of 30 arc-sec (Weatherall et al. 2015). The model includes bottom friction and the Coriolis forces and solves the shallow-water equations over a spherical domain. This numerical model was successfully applied for the modeling of a number of large tsunamis including the 2011 Tohoku (Japan) tsunami (Satake et al. 2013; Satake 2014). A time step of 1.0 s was used for linear simulations. Tsunami simulations were initiated using coseismic seafloor deformations obtained from the Okada's (1985) analytical solution for coseismic dislocation.

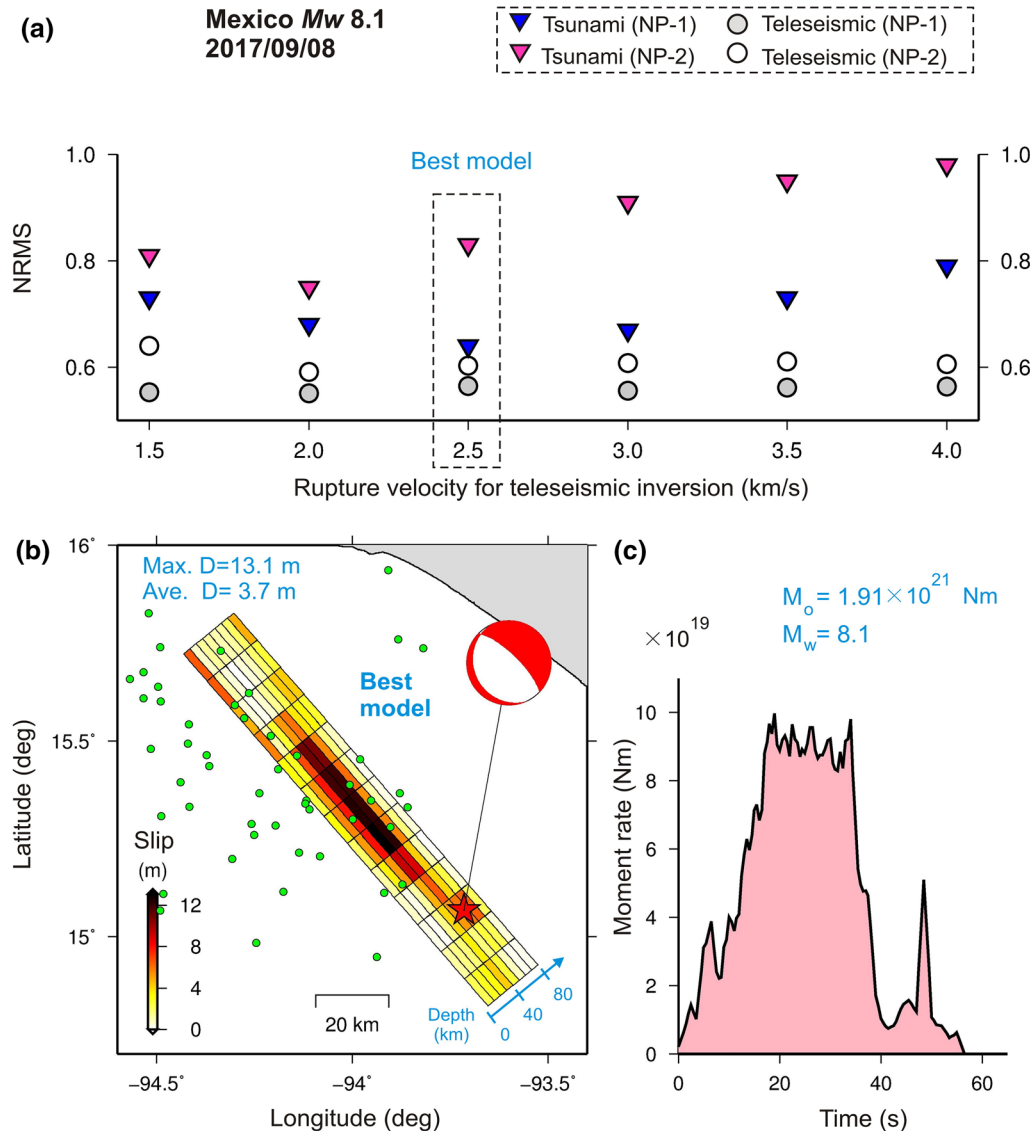


Figure 2

a NRMS misfits for teleseismic inversions and tsunami simulations for various slip models of the 8 September 2017 Chiapas earthquake. **b** Best source model belonging to NP-1 and $V_r = 2.5$ km/s. **c** Moment-rate (source-time) function for the best source model

The quality of fit between observations and simulations was measured by using the normalized root mean square (NRMS) misfit equation of Heidarzadeh et al. (2016a, b).

Since the 2017 Chiapas earthquake occurred within the Tehuantepec seismic gap, potential stress transfer to the neighboring areas and its effects on regional future seismicity are of great concern. In this context, we calculated static changes in the Coulomb stress (ΔCFF) due to the 2017 Chiapas earthquake on

the plate interface between the Cocos and the North American plates. ΔCFF was obtained using the following equation:

$$\Delta CFF = \Delta\tau - \mu' \Delta\sigma,$$

in which μ' denotes the apparent friction coefficient, $\Delta\tau$ is the shear stress changes, and $\Delta\sigma$ is the normal stress change (Ishibe et al. 2015, 2017; Stein et al. 1992). The sign of ΔCFF indicates increase (for positive values) or decrease (for negative values) in

Slip distributions for the steep fault plane (NP-1)

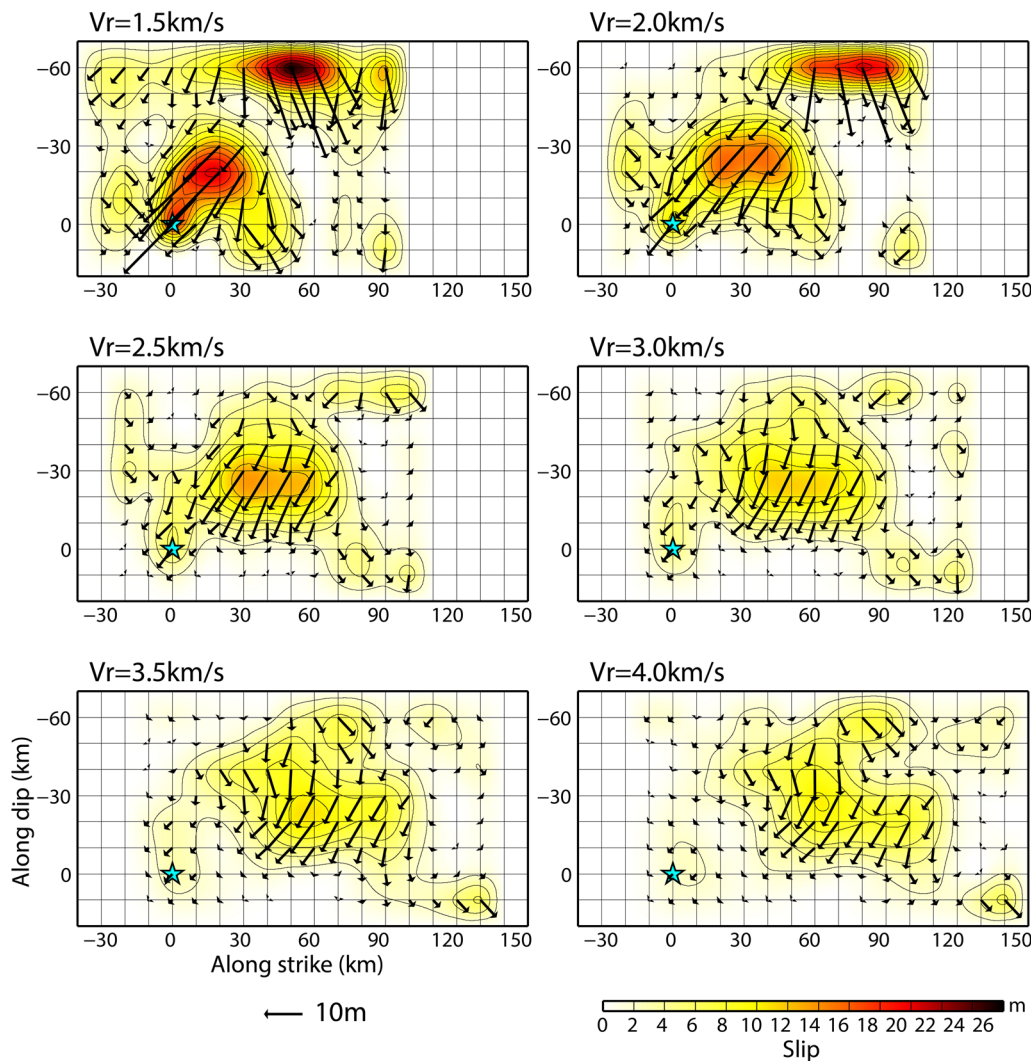


Figure 3

Various slip distributions from the steep fault plane (NP-1) for the 8 September 2017 Chiapas, Mexico M_w 8.1 earthquake considering different rupture velocity (V_r) from 1.5 km/s to 4.0 km/s

Coulomb stress for the neighboring areas imparted by the mainshock. The slip model obtained in this study for the 2017 Chiapas earthquake was used for the ΔCFF analysis assuming $\mu' = 0.4$, Poisson ratio = 0.25 and earth's rigidity = 40 GPa. The receiver fault parameters were: strike angle, 296° ; dip angle, 14° ; rake angle, 70° . We used a three-dimensional compilation of global subduction geometries (slab 1.0; Hayes et al. 2012) as the calculation depth.

3. Finite-Fault Slip Model

We first obtained 12 slip distributions for NP-1 and NP-2 by finite-fault teleseismic inversions whose NRMS misfits are shown in Fig. 2a. Different slip distributions and source-time functions are presented in Figs. 3, 4, 5 and 6, while Figure S2 (in the supporting information) shows an example of match between the observed and synthetic teleseismic waveforms. The rupture length was increased as V_r increased from 1.5 to 4.0 km/s (Figs. 3, 5). Based on

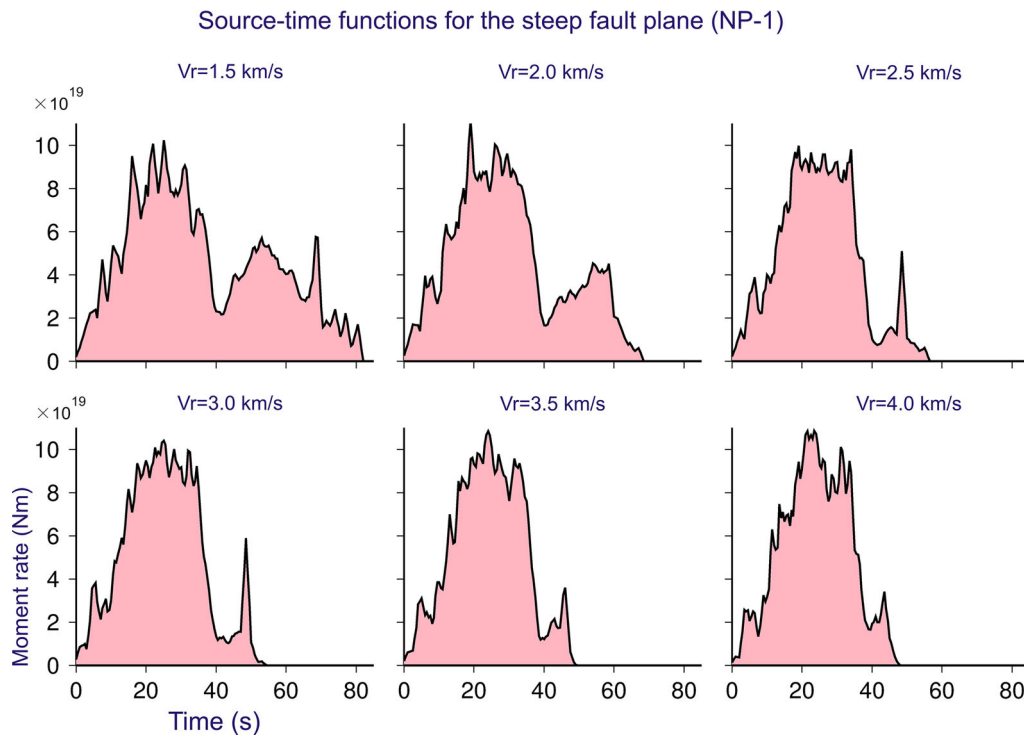


Figure 4

Various source-time functions (moment-rate functions) from the steep fault plane (NP-1) for the 8 September 2017 Chiapas, Mexico M_w 8.1 earthquake considering different rupture velocities (V_r) from 1.5 km/s to 4.0 km/s

Fig. 4, a trade-off was seen between rupture duration of the earthquake, and the V_r : duration decreased from 82.0 s for $V_r = 1.5$ km/s to 48.0 s for $V_r = 4.0$ km/s. The NRMS misfit from teleseismic inversions indicated that the synthetic waveforms from NP-1 produce better agreements with observations than NP-2. For all V_r , the misfit values from NP-1 are smaller than those from NP-2. Therefore, results of teleseismic inversion clearly favor NP-1 over NP-2. However, the misfits obtained for various V_r (within NP-1) are close to each other preventing an effective selection of the best model (Fig. 2a). The NRMS misfits by teleseismic inversions for NP-1 are in the range of 0.5507–0.5650, indicating 2.5% of misfit change between the lower and the upper limits. Therefore, it was not straightforward to choose the best slip model out of the six models from NP-1.

Tsunami simulations were conducted for all 12 slip distributions from NP-1 and NP-2 to further constrain the earthquake source. According to Figs. 2a, 7 and 8, tsunami simulations also favor NP-

1 over NP-2. The tsunami NRMS misfits were calculated for the first tsunami waves as shown by blue lines on top of the tsunami waveforms in Figs. 7 and 8. The NRMS misfits from tsunami simulations for NP-1 are meaningfully separated from each other ranging from 0.64 to 0.79, which gives a misfit change of 19%. The minimum value for the NP-1 misfits occurs at the $V_r = 2.5$ km/s and the misfit values increase toward both sides of this V_r . According to Fig. 2a, the best source model is the one with $V_r = 2.5$ km/s from NP-1. Figure 7 shows the results of tsunami simulations and comparison with observations for the best source model indicating good quality of match between tsunami observations and simulations for most of the stations, especially for the DART stations. At some tsunami stations (e.g., Acapulco-CDY and Huatulco), the quality of match looks poor which can be possibly attributed to the insufficient quality of bathymetry data used for tsunami simulations (e.g., Okal et al. 2009; Heidarzadeh et al. 2016a, 2017b; Heidarzadeh and

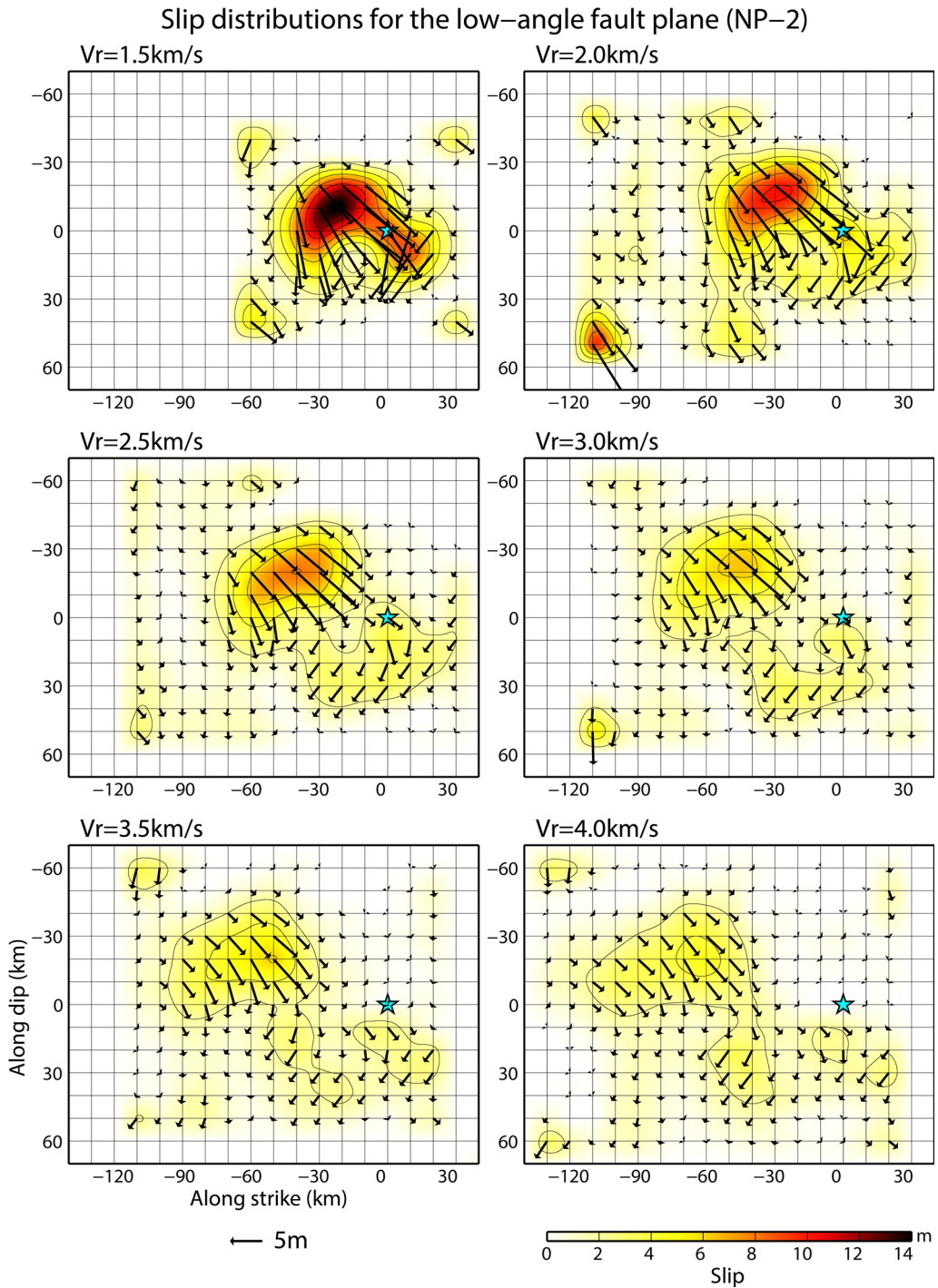


Figure 5

Various slip distributions from the low-angle fault plane (NP-2) for the 8 September 2017 Chiapas, Mexico M_w 8.1 earthquake considering different rupture velocities (V_r) from 1.5 km/s to 4.0 km/s

Source-time functions for the low-angle fault plane (NP-2)

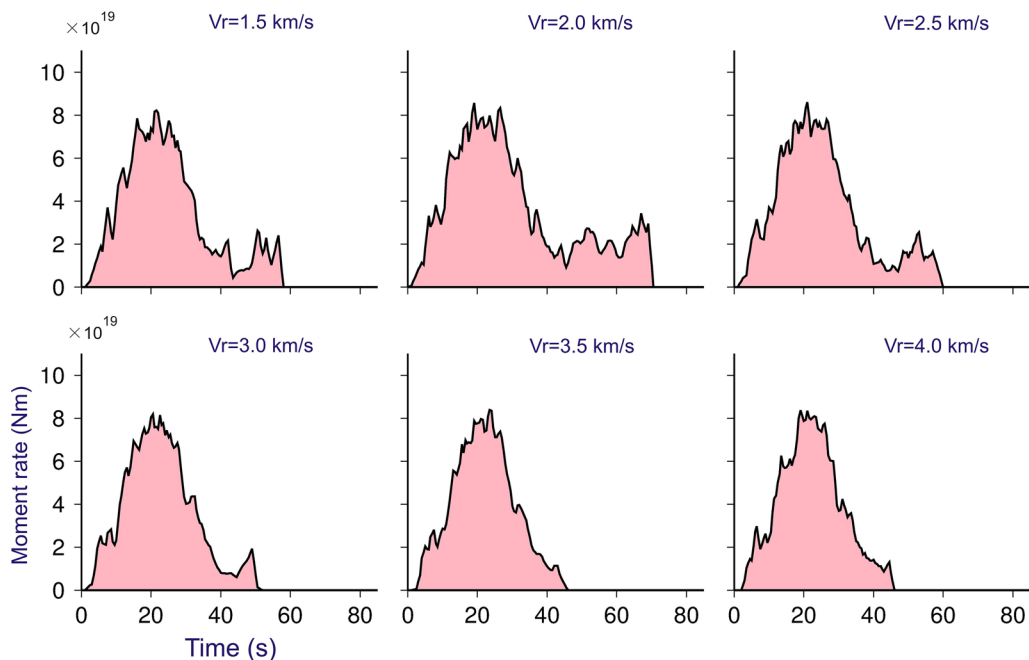


Figure 6

Various source-time functions (moment-rate functions) from the low-angle fault plane (NP-2) for the 8 September 2017 Chiapas, Mexico M_w 8.1 earthquake considering different rupture velocities (V_r) from 1.5 km/s to 4.0 km/s

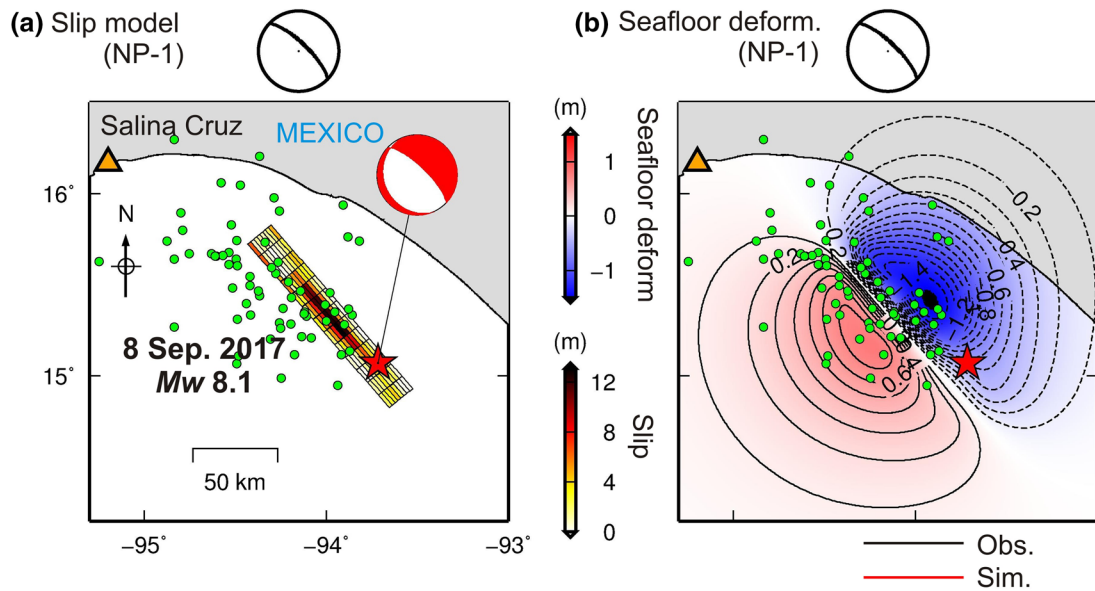
Satake 2017). Most tide gauges are located inside harbors with harbor opening of 100–300 m. Therefore, accurate modeling of tide gauge records requires high-resolution bathymetric data with grid spacing of 100 m or less (e.g., Rabinovich 2009; Heidarzadeh and Satake 2014). While our numerical model was capable of reproducing most tide gauge records of the 2017 Mexico tsunami, the lack of success in Acapulco-CDY and Huatulco can be due to the small opening of these two harbors. For example, the opening of the Huatulco harbor is ~ 200 m. Lack of good match in some other tsunami stations (e.g., La Libertad_ES and Callao) is possibly due to low signal to noise ratio (i.e., small size of the tsunami with high noise levels) in these stations. For comparison, we plotted the simulation results for $V_r = 2.0$ km/s from NP-2, producing the smallest NRMS for NP-2, in Fig. 8.

The best finite-fault slip model, based on teleseismic body-wave inversions and forward tsunami

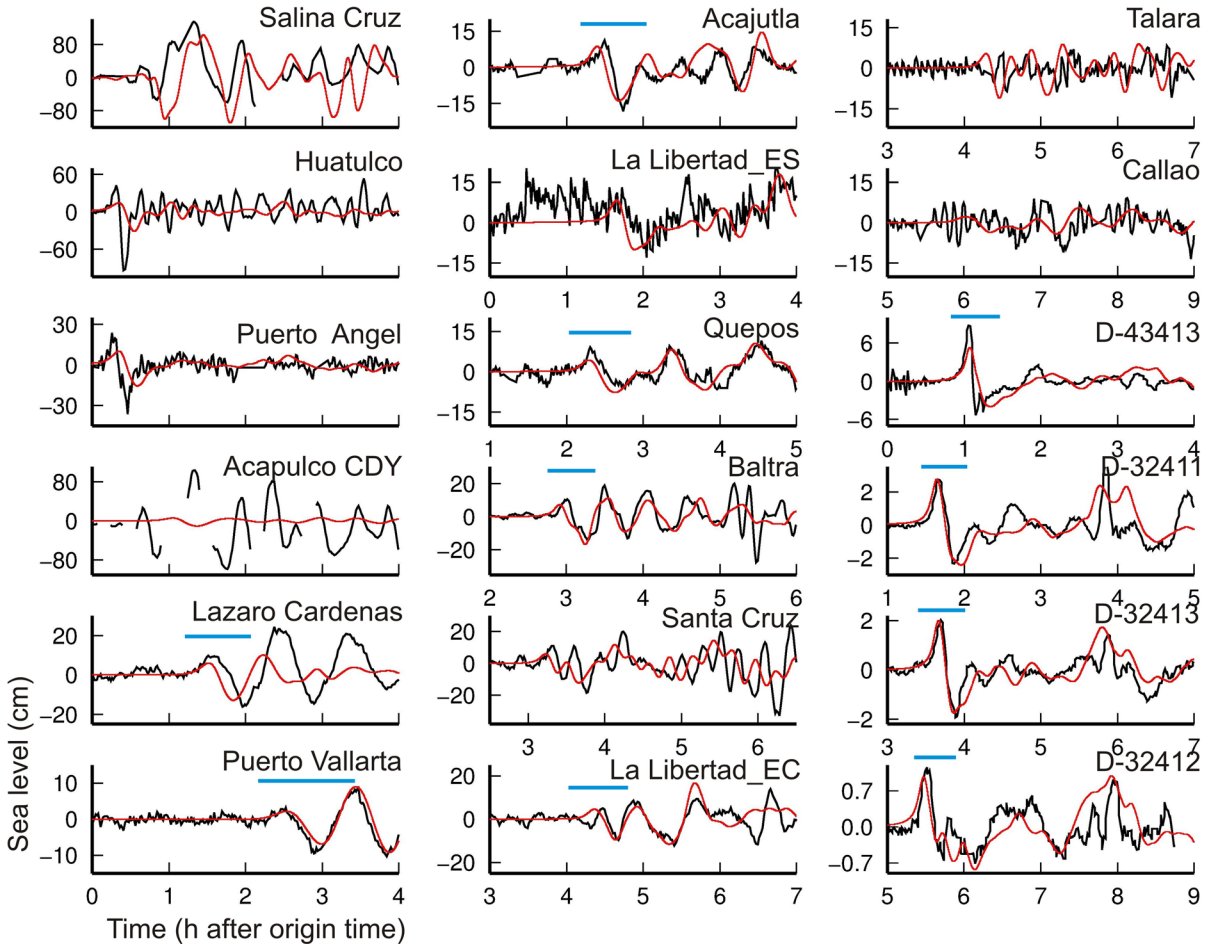
Figure 7

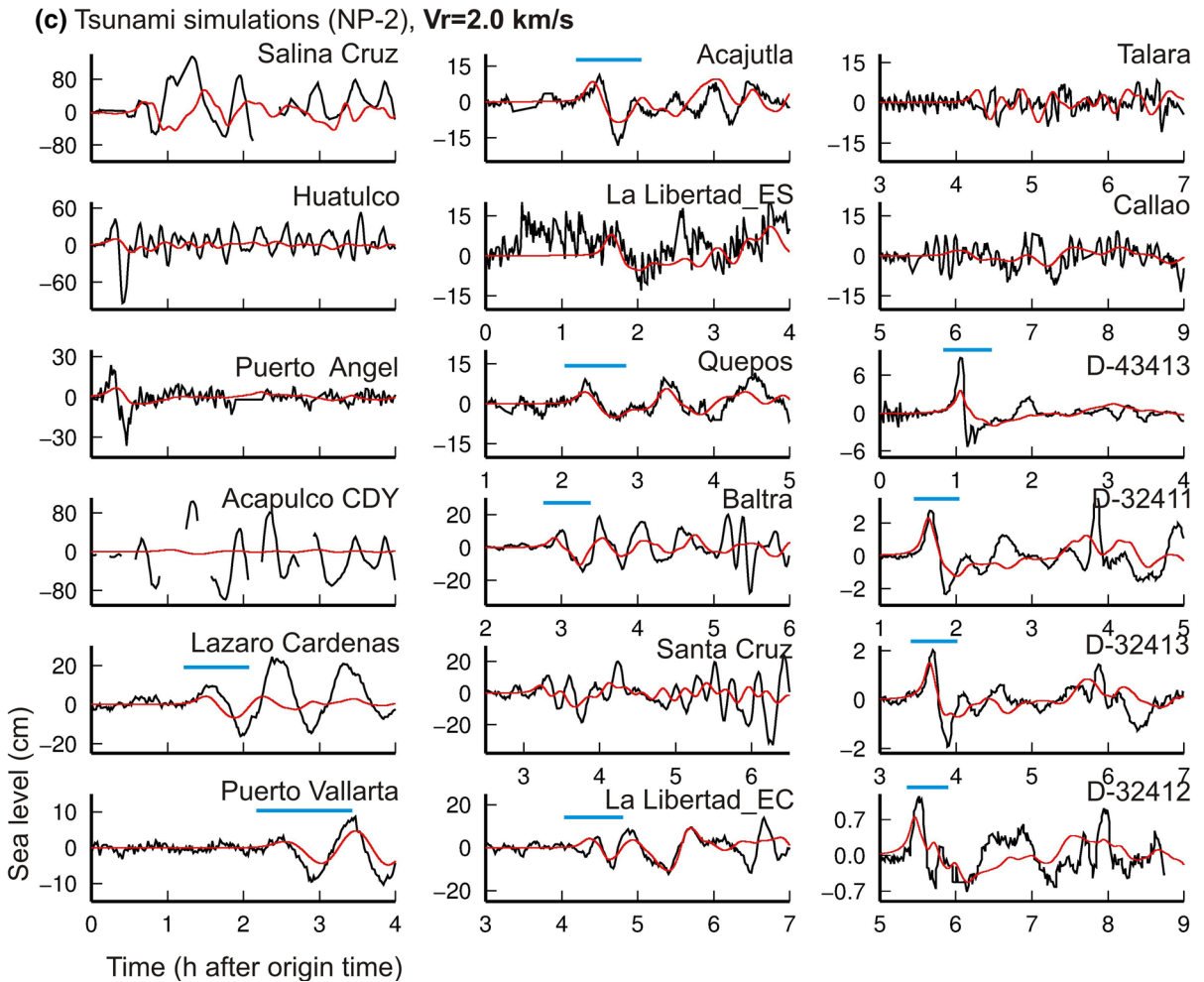
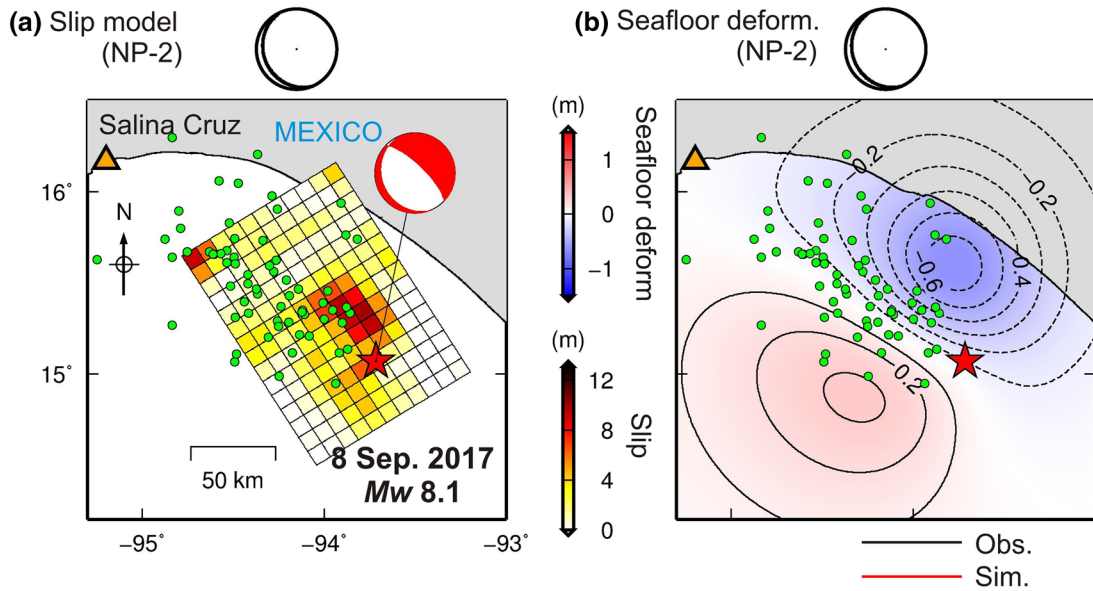
a Slip distribution for the 8 September 2017 Chiapas earthquake for NP-1 and $V_r = 2.5$ km/s which is the best source model. Green circles are 1-day aftershocks based on the USGS catalog. The triangle shows the Salina Cruz tide gauge station. **b** Coseismic seafloor deformation for uplift (solid lines) and subsidence (dashed lines) at 0.1 m intervals. **c** Observed (black) and simulated (red) tsunami waveforms. See Fig. 1 for locations of the tsunami stations. The blue lines on top of some of the waveforms show part of the waveforms used for NRMS misfit calculations

simulations, belongs to the NP-1 (i.e., steep fault plane) with $V_r = 2.5$ km/s. The dimension of the fault is 130 km in length \times 80 km in width, with maximum and average slip amounts of 13.1 and 3.7 m (Fig. 2b). The main rupture unilaterally propagates toward northwest and the large slip patch (slip = 7–13 m) is located at the depth range of 30–50 km. The duration of the earthquake rupture was 56.5 s and the seismic moment was estimated to



(c) Tsunami simulations (NP-1), $V_r=2.5$ km/s





◀ Figure 8

a Slip distribution for the 8 September 2017 Chiapas earthquake for NP-2 and $V_r = 2.0$ km/s. Green circles are 1-day aftershocks based on the USGS catalog. The triangle shows the Salina Cruz tide gauge station. **b** Coseismic seafloor deformation for uplift (solid lines) and subsidence (dashed lines) at 0.1 m intervals. **c** Observed (black) and simulated (red) tsunami waveforms. See Fig. 1 for locations of the tsunami stations. The blue lines on top of some of the waveforms show part of the waveforms used for NRMS misfit calculations

be 1.91×10^{21} Nm giving $M_w = 8.1$. Our source model obtained from joint tsunami and teleseismic data is consistent with that of Gusman et al. (2018) and Adriano et al. (2018), which are based on tsunami inversion.

4. Stress Transfer from the 2017 Chiapas Earthquake

The source region of the 2017 Chiapas earthquake is located within the Tehuantepec seismic gap zone along offshore Mexico; hence, the effect of the 2017 Chiapas earthquake on future potential induced-seismicity in this seismic zone would be of great concern. Thus, we calculated the static Coulomb stress changes on the thrust-focal-mechanism earthquakes imparted by the 2017 Chiapas earthquake (Figs. 9 and S3). The positively stressed region is mainly distributed in the shallower part of the Tehuantepec gap (i.e., near the trench axis), while the Δ CFF values are negative for the deeper part (i.e., along the

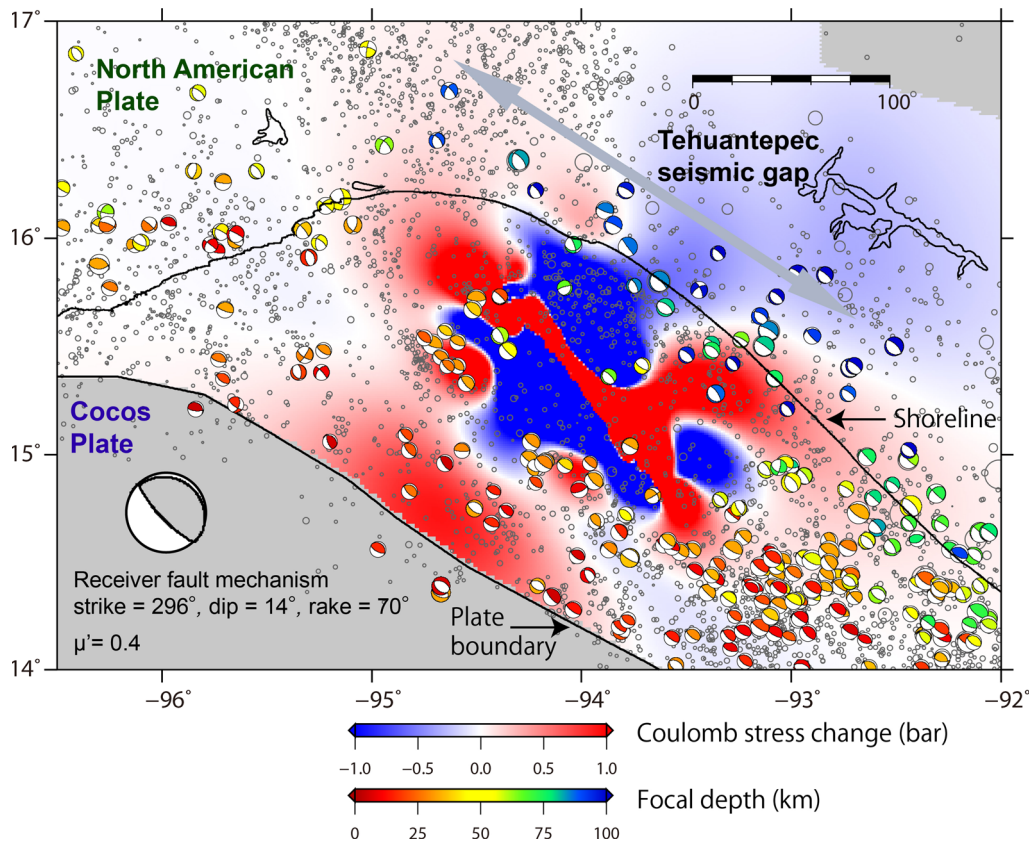


Figure 9

Results of Δ CFF analysis from the 2017 Chiapas earthquake for the plate interface between the Cocos plate and North American plate with the receiver fault mechanism (strike: 296°, dip: 14°, rake: 70°) considering apparent friction coefficient (μ') of 0.4. The focal mechanism solution is from the GCMT catalog for the period from January 1976 to before the mainshock (i.e., September 8, 2017). The depth range is 0–100 km. Gray circles are epicenter distribution of earthquakes from the USGS catalog for the time period from January 2000 to before the mainshock. Star represents the epicenter of the 2017 Chiapas earthquake

shoreline). According to Fig. 9, the Δ CFE analysis implies that this normal-faulting intraplate earthquake might have increased the stress at the offshore region of the Tehuantepec gap (i.e., near the trench), which can indicate future earthquake possibilities. In other words, the 2017 Chiapas intraplate earthquake could facilitate future large thrust-fault interplate earthquakes in this region. Concerning regional seismicity, Segou and Parsons (2018) showed that the occurrence of the 2017 M_w 8.1 Chiapas earthquake and some of its $M > 7$ aftershocks was facilitated by past large thrust earthquakes in this region. The stress transfer analysis following the Chiapas earthquake by Stein et al. (2017) also revealed zones with increased stress at the plate boundary.

5. Conclusions

The 8 September 2017 Chiapas earthquake was analyzed by applying teleseismic body-wave inversion, forward tsunami simulations and the Coulomb stress transfer analysis. The main results are:

1. The maximum tide gauge and DART zero-to-crest tsunami amplitudes, among the observed data, were 133.8 cm (Salina Cruz) and 8.8 cm (DART 43413) for the 2017 Chiapas tsunami, respectively.
2. To resolve the actual fault plane between the steep (NP-1) and low-angle (NP-2) nodal planes, teleseismic inversions were performed for both nodal planes employing rupture velocities (V_r) of 1.5–4.0 km/s. While teleseismic inversions favored NP-1 over NP-2, it was not possible to select the best V_r .
3. Tsunami simulations revealed that NP-1 is a better fault plane than NP-2 in terms of agreement between tsunami observations and simulations and conclusively guided the selection of $V_r = 2.5$ km/s as the best source model. We report a source model with dimensions of 130 km (strike-wise) \times 80 km (dip-wise), maximum and average slips of 13.1 and 3.7 m, respectively, belonging to the steep fault plane (NP-1). Duration of the earthquake, seismic moment and M_w were 56.5 s, 1.91×10^{21} Nm and 8.1, respectively.
4. Coulomb stress transfer analysis revealed that the shallower part of the Tehuantepec gap (i.e., near the trench axis) received positive stress, while negative stress was transferred to the deeper part (i.e., along the shoreline). The probabilities for the occurrence of future large thrust interplate earthquakes in the region may have been increased following the 2017 Chiapas M_w 8.1 intraplate earthquake.

Acknowledgements

Tsunami DART data used here came from the US National Oceanic and Atmospheric Administration (NOAA) website (<http://www.ndbc.noaa.gov/dart.shtml>). Tide gauge data were downloaded from Intergovernmental Oceanographic Commission website (<http://www.iocsealevelmonitoring.org/>). We obtained teleseismic data for inversions from the Incorporated Research Institutions for Seismology (http://www.iris.edu/wilber3/find_event). We used The GMT software by Wessel and Smith (1998) in this study. MH is grateful to the Brunel University London for the funding provided through the Brunel Research Initiative and Enterprise Fund 2017/18 (BUL BRIEF). The authors declare that they have no competing interests regarding the work presented in this article. We are grateful to two anonymous reviewers.

Open Access This article is distributed under the terms of the Creative Commons Attribution 4.0 International License (<http://creativecommons.org/licenses/by/4.0/>), which permits unrestricted use, distribution, and reproduction in any medium, provided you give appropriate credit to the original author(s) and the source, provide a link to the Creative Commons license, and indicate if changes were made.

REFERENCES

- Adriano, B., Fujii, Y., Koshimura, S., Mas, E., Ruiz-Angulo, A., & Estrada, M. (2018). Tsunami source inversion using tide gauge and DART tsunami waveforms of the 2017 M_w 8.2 Mexico earthquake. *Pure and Applied Geophysics*, 175, 33–48.
- Gusman, A. R., Mulia, I. E., & Satake, K. (2018). Optimum sea surface displacement and fault slip distribution of the 2017

- Tehuantepec earthquake (M_w 8.2) in Mexico estimated from tsunami waveforms. *Geophysical Research Letters*. <https://doi.org/10.1002/2017GL076070>.
- Gusman, A. R., Murotani, S., Satake, K., Heidarzadeh, M., Gunawan, E., Watada, S., et al. (2015). Fault slip distribution of the 2014 Iquique, Chile, earthquake estimated from ocean-wide tsunami waveforms and GPS data. *Geophysical Research Letters*, 42, 1053–1060. <https://doi.org/10.1002/2014GL062604>.
- Gusman, A. R., Satake, K., Shinohara, M., Sakai, S., & Tanioka, Y. (2017). Fault slip distribution of the 2016 Fukushima earthquake estimated from tsunami waveforms. *Pure and Applied Geophysics*. <https://doi.org/10.1007/s00024-017-1590-2>.
- Hatori, T. (1995). Magnitude scale for the Central American tsunamis. *Pure and Applied Geophysics*, 144(3), 471–479.
- Hayes, G. P., Wald, D. J., & Johnson, R. L. (2012). Slab1.0: A three-dimensional model of global subduction zone geometries. *Journal of Geophysical Research*, 117, B01302. <https://doi.org/10.1029/2011JB008524>.
- Heidarzadeh, M., Harada, T., Satake, K., Ishibe, T., & Gusman, A. R. (2016a). Comparative study of two tsunamigenic earthquakes in the Solomon Islands: 2015 M_w 7.0 normal-fault and 2013 Santa Cruz M_w 8.0 megathrust earthquakes. *Geophysical Research Letters*, 43, 4340–4349.
- Heidarzadeh, M., Harada, T., Satake, K., Ishibe, T., & Takagawa, T. (2017a). Tsunamis from strike-slip earthquakes in the Wharton Basin, northeast Indian Ocean: March 2016 M_w 7.8 event and its relationship with the April 2012 M_w 8.6 event. *Geophysical Journal International*, 211(3), 1601–1612.
- Heidarzadeh, M., Murotani, S., Satake, K., Ishibe, T., & Gusman, A. R. (2016b). Source model of the 16 September 2015 Illapel, Chile M_w 8.4 earthquake based on teleseismic and tsunami data. *Geophysical Research Letters*, 43, 643–650.
- Heidarzadeh, M., Murotani, S., Satake, K., Takagawa, T., & Saito, T. (2017b). Fault size and depth extent of the Ecuador earthquake (M_w 7.8) of 16 April 2016 from teleseismic and tsunami data. *Geophysical Research Letters*, 44, 2211–2219.
- Heidarzadeh, M., & Satake, K. (2014). Possible sources of the tsunami observed in the northwestern Indian Ocean following the 2013 September 24 M_w 7.7 Pakistan inland earthquake. *Geophysical Journal International*, 199(2), 752–766.
- Heidarzadeh, M., & Satake, K. (2017). Possible dual earthquake-landslide source of the 13 November 2016 Kaikoura, New Zealand tsunami. *Pure and Applied Geophysics*, 174(10), 3737–3749.
- Ishibe, T., Ogata, Y., Tsuruoka, H., & Satake, K. (2017). Testing the Coulomb stress triggering hypothesis for three recent megathrust earthquakes. *Geoscience Letters*, 4, 5. <https://doi.org/10.1186/s40562-017-0070-y>.
- Ishibe, T., Satake, K., Sakai, S., Shimazaki, K., Tsuruoka, H., Yokota, Y., et al. (2015). Correlation between Coulomb stress imparted by the 2011 Tohoku-Oki earthquake and seismicity rate change in Kanto, Japan. *Geophysical Journal International*, 201(1), 112–134.
- Kennett, B. L. N., Engdahl, E. R., & Buland, R. (1995). Constraints on seismic velocities in the Earth from travel times. *Geophysical Journal International*, 122, 108–124.
- Laske, G., Masters, G., Ma, Z., Pasyanos, M. (2013). Update on CRUST1.0-A 1-degree Global Model of Earth's Crust. In *Geophysical Research Abstracts*, 15, Abstract EGU2013-2658.
- Lay, T., Yue, H., Brodsky, E. E., & An, C. (2014). The 1 April 2014 Iquique, Chile, M_w 8.1 earthquake rupture sequence. *Geophysical Research Letters*, 41, 3818–3825.
- Okada, Y. (1985). Surface deformation due to shear and tensile faults in a half-space. *Bulletin of the Seismological Society of America*, 75, 1135–1154.
- Okal, E. A., & Synolakis, C. E. (2004). Source discriminants for near-field tsunamis. *Geophysical Journal International*, 158(3), 899–912.
- Okal, E. A., Synolakis, C. E., Uslu, B., Kalligeris, N., & Voukouvalas, E. (2009). The 1956 earthquake and tsunami in Amorgos, Greece. *Geophysical Journal International*, 178(3), 1533–1554.
- Ortiz, M., Singh, S. K., Kostoglodov, V., & Pacheco, J. (2000). Source areas of the Acapulco-San Marcos, Mexico earthquakes of 1962 (M 7.1; 7.0) and 1957 (M 7.7), as constrained by tsunami and uplift records. *Geofísica Internacional*, 39(4), 337–348.
- Ortiz, M., Singh, S. K., Pachecoand, J., & Kostoglodov, V. (1998). Rupture length of the October 9, 1995 Colima-Jalisco Earthquake (M_w 8) estimated from tsunami data. *Geophysical Research Letters*, 25(15), 2857–2860.
- Rabinovich, A.B. (2009). Seiches and Harbor Oscillations. In: *Handbook of Coastal and Ocean Engineering* (pp. 193–236).
- Rabinovich, A. B., Lobkovsky, L. I., Fine, I. V., Thomson, R. E., Ivelskaya, T. N., & Kulikov, E. A. (2008). Near-source observations and modeling of the Kuril Islands tsunamis of 15 November 2006 and 13 January 2007. *Advances in Geosciences*, 14, 105–116.
- Ramírez-Herrera, M. T., Corona, N., Ruiz-Angulo, A., Melgar, D., & Zavala-Hidalgo, J. (2018). The 8 September 2017 Tsunami Triggered by the M_w 8.2 Intraplate Earthquake, Chiapas, Mexico. *Pure and Applied Geophysics*, 175, 25–34.
- Satake, K. (1995). Linear and nonlinear computations of the 1992 Nicaragua earthquake tsunami. *Pure and Applied Geophysics*, 144, 455–470.
- Satake, K. (2014). Advances in earthquake and tsunami sciences and disaster risk reduction since the 2004 Indian ocean tsunami. *Geoscience Letters*, 1(1), 15.
- Satake, K., Fujii, Y., Harada, T., & Namegaya, Y. (2013). Time and space distribution of coseismic slip of the 2011 Tohoku earthquake as inferred from tsunami waveform data. *Bulletin of the Seismological Society of America*, 103(2B), 1473–1492.
- Segou, M., & Parsons, T. (2018). Testing earthquake links in Mexico from 1978 up to the 2017 $M = 8.1$ Chiapas and $M = 7.1$ Puebla shocks. *Geophysical Research Letters*, 45, 708–714.
- Singh, S. K., Astiz, L., & Havskov, J. (1981). Seismic gaps and recurrence periods of large earthquakes along the Mexican subduction zone: a reexamination. *Bulletin of the Seismological Society of America*, 71(3), 827–843.
- Singh, S. K., Havskov, J., McNally, K., Ponce, L., Hearsh, T., & Vassiliou, M. (1980). The Oaxaca Mexico, Earthquake of 29 November 1978: a preliminary report on aftershocks. *Geofísica Internacional*, 17(3), 335–340.
- Stein, R. S., King, G. C. P., & Lin, J. (1992). Change in failure stress on the southern San Andreas fault system caused by the 1992 magnitude = 7.4 Landers earthquake. *Science*, 258, 1328–1332.
- Stein, R., Toda, S., Ely, G., Jacobson, D. (2017). Are Mexico's two major earthquakes related, and what could happen next?. <http://temblor.net/earthquake-insights/are-mexicos-two-major-earthquakes-related-and-what-could-happen-next-5149/>.

- Synolakis, C. E., & Okal, E. A. (2005). 1992-2002: Perspective on a decade of post-tsunami surveys. In: K. Satake, Tsunami. *Advances in Natural and Technological Hazards Research*, 23, 1–30.
- Weatherall, P., Marks, K. M., Jakobsson, M., Schmitt, T., Tani, S., Arndt, J. E., et al. (2015). A new digital bathymetric model of the world's oceans. *Earth and Space Science*, 2, 331–345. <https://doi.org/10.1002/2015EA000107>.
- Wessel, P., & Smith, W. H. F. (1998). New, improved version of generic mapping tools released. *EOS Transaction AGU*, 79(47), 579. <https://doi.org/10.1029/98EO00426>.
- Zhang, H., Koper, K. D., Pankow, K., & Ge, Z. (2017). Imaging the 2016 M_w 7.8 Kaikoura, New Zealand, earthquake with teleseismic P waves: A cascading rupture across multiple faults. *Geophysical Research Letters*. <https://doi.org/10.1002/2017GL073461>.

(Received January 17, 2018, revised March 7, 2018, accepted March 9, 2018, Published online April 9, 2018)